iScience

CellPress
OPEN ACCESS

Article

Single-cell transcriptomic mapping of intestinal epithelium that undergoes 3D morphogenesis and mechanodynamic stimulation in a gut-on-a-chip

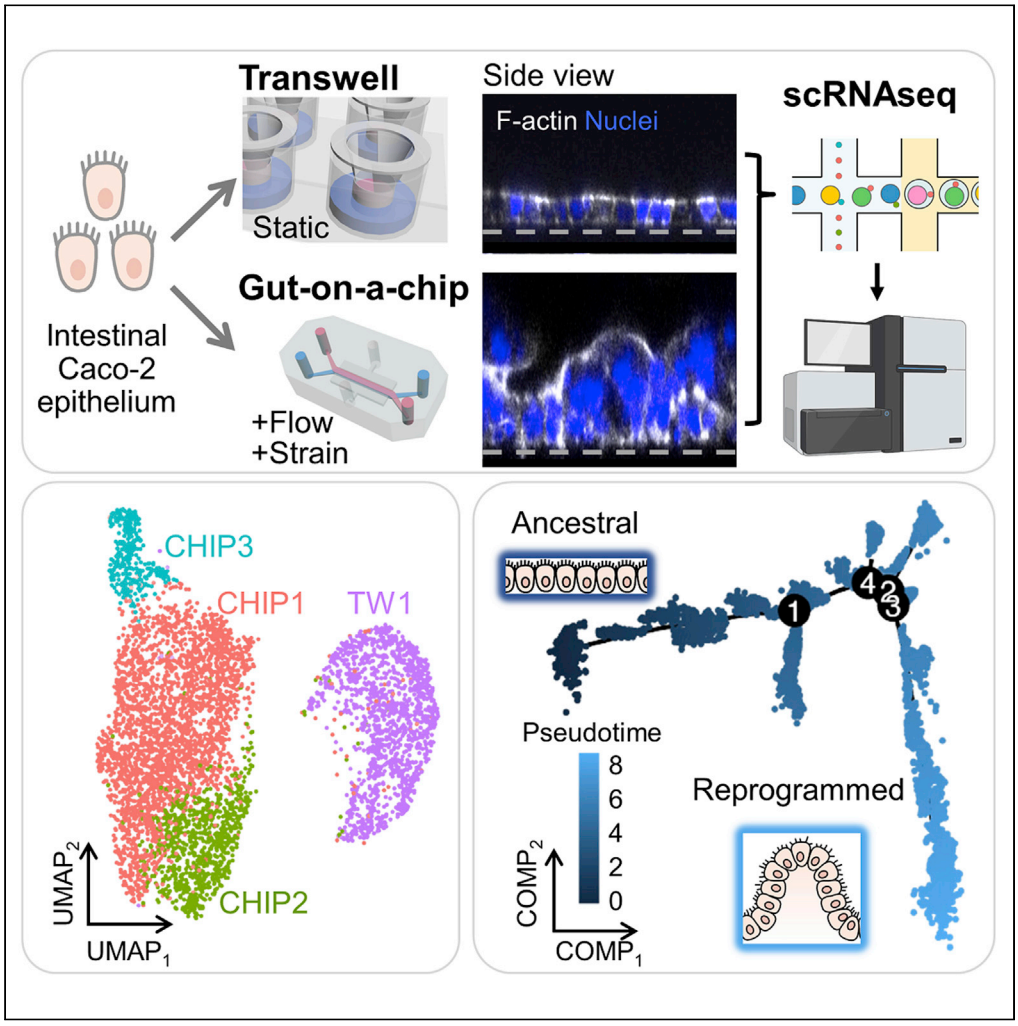

Woojung Shin, Zhe Su, S. Stephen Yi, Hyun Jung Kim

stephen.yi@austin.utexas.edu (S.S.Y.)
kimh19@ccf.org (H.J.K.)

Highlights

Gut-on-a-chip cultures induce the mechanodynamic stimulation of Caco-2 epithelium

Single-cell transcriptomics confirms spatial mapping of reprogrammed Caco-2 cells

Pseudotemporal evolution of Caco-2 perturbs intestinal functions and drug metabolism

Microphysiological on-chip cultures reprogram cancer inheritance of Caco-2 cells

Shin et al., iScience 25, 105521
December 22, 2022
https://doi.org/10.1016/j.isci.2022.105521

iScience

CellPress
OPEN ACCESS

Article

Single-cell transcriptomic mapping of intestinal epithelium that undergoes 3D morphogenesis and mechanodynamic stimulation in a gut-on-a-chip

Woojung Shin,[1,2,3,7] Zhe Su,[4,7] S. Stephen Yi,[3,4,5,*] and Hyun Jung Kim[3,4,6,8,*]

SUMMARY

The human gut-on-a-chip has demonstrated *in vivo*-relevant cellular fidelity and physiological functions of Caco-2 intestinal epithelium compared to its static cultures. However, transcriptomic dynamics that controls the morphogenic and mechanodynamic perturbation of Caco-2 epithelium in a microphysiological culture remain elusive. Single-cell transcriptomic analysis revealed that a gut-on-a-chip culture drives three clusters that illustrate distinct gene expressions and their spatial representation in three-dimensional (3D) epithelial layers. A pseudotemporal trajectory analysis elucidated the evolutionary transition from a homogeneous ancestral genotype in Transwell cultures into heterogeneous transcriptomes in gut-on-a-chip cultures, verified in cell cycle perturbation, cytodifferentiation, and intestinal functions in digestion, transport, and drug metabolism. Furthermore, the inversed transcriptomic signature of oncogenes and tumor-suppressor genes of Caco-2 cells confirmed that gut-on-a-chip cultures induce postmitotic reprogramming of cancer-associated genes. Our study suggests that a physiological gut-on-a-chip culture induces the transcriptomic perturbation of Caco-2 epithelium to elicit *in vivo*-relevant morphogenesis and restoration of normal physiological functions.

INTRODUCTION

The Caco-2 human colon adenocarcinoma line has been extensively used as a gold standard for estimating the intestinal permeability of drugs in pharmaceutical validation over the past decades.[1–3] The Caco-2 epithelium has enterocyte-like phenotypes with transcriptomic signatures of normal small intestinal epithelium when cultured for 2-3 weeks in a static condition despite its cancer origin.[4–6] However, Caco-2 cells cultured as a 2D monolayer have shown a considerable deficiency in physiological 3D morphology, cytodifferentiation, and essential intestinal functions, including drug metabolism and mucus production.[7] Notably, epithelial cultures in a gut-on-a-chip induce the cytodifferentiation and histogenesis of Caco-2 cells under mechanodynamic fluid shear stress and physical deformations.[8–10] Notably, the biochemical gradient and mechanical cues reprogram the phenotypic features, including spontaneous 3D morphogenesis,[8,10,11] lineage-dependent differentiation, mucus production, drug metabolism,[9] and flow-dependent modulation of canonical Wnt signaling and subsequent subcellular morphogenic responses.[10] These observations suggest that the phenotypic reprogramming of Caco-2 cells is remarkable when the cells undergo microphysiological manipulation during gut-on-a-chip cultures. However, the transcriptomic perturbation pertinent to phenotypic reprogramming of the Caco-2 epithelium has not been sufficiently investigated in a single-cell resolution.

In this study, we applied the single-cell RNA sequencing (scRNA-seq) method to compare the transcriptome profiles of Caco-2 cells cultured in either a gut-on-a-chip or a static Transwell insert to verify how the mechanodynamic on-chip cultures perturb epithelial transcriptomic dynamics that lead to cytohistological and functional reprogramming of intestinal epithelium. We examined the heterogeneity of cell populations depending on the culture formats by dimensionality reduction, spatial mapping of the selected genes visualized on 3D epithelial layers, and pseudotemporal trajectory analysis. We also discovered significant transcriptomic perturbations of Caco-2 cells associated with intestinal epithelial function, differentiation, and drug transport and metabolism during on-chip cultures. Finally, the reversion of cancer-specific signatures in Caco-2 cells

[1]Wyss Institute for Biologically Inspired Engineering, Harvard University, Boston, MA 02115, USA

[2]Institute for Medical Engineering and Science, Massachusetts Institute of Technology, Cambridge, MA 02139, USA

[3]Department of Biomedical Engineering, The University of Texas at Austin, Austin, TX 78712, USA

[4]Department of Oncology, Livestrong Cancer Institutes, Dell Medical School, The University of Texas at Austin, Austin, TX 78712, USA

[5]Oden Institute for Computational Engineering and Sciences (ICES), and Interdisciplinary Life Sciences Graduate Programs (ILSGP), The University of Texas at Austin, Austin, TX 78712, USA

[6]Department of Inflammation and Immunity, Lerner Research Institute, Cleveland Clinic, Cleveland, OH 44195, USA

[7]These authors contributed equally

[8]Lead contact

*Correspondence: stephen.yi@austin.utexas.edu (S.S.Y.), kimh19@ccf.org (H.J.K.)

https://doi.org/10.1016/j.isci.2022.105521

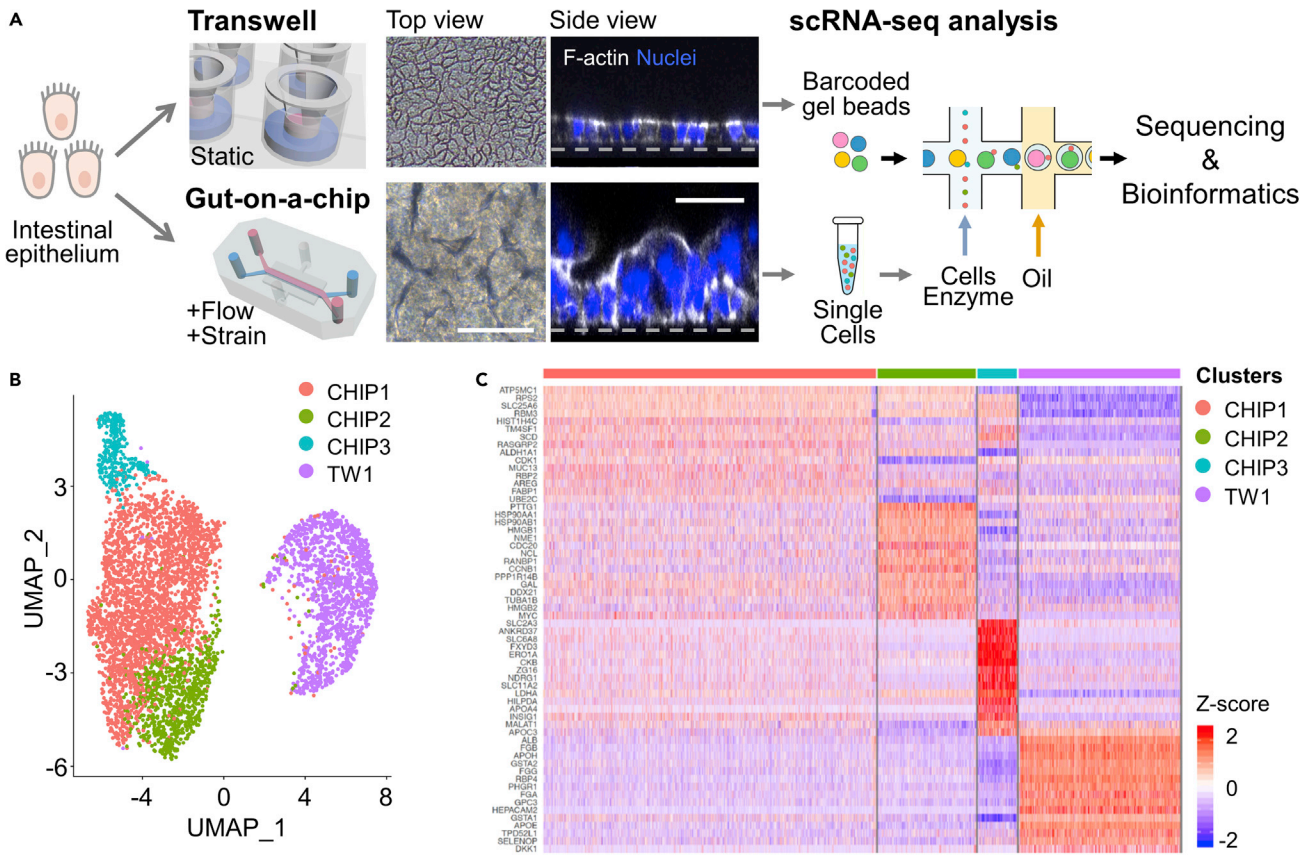

Figure 1. Single-cell transcriptomic characterization of culture-dependent epithelial heterogeneity

(A) An overview of the experimental scRNA-seq analysis of Caco-2 cells cultured in either a static Transwell or a mechanodynamic gut-on-a-chip. Caco-2 cells cultured in a Transwell insert formed a 2D monolayer, whereas the same cells cultured in a gut-on-a-chip under flow and stretching motions regenerated a 3D villi-like epithelial microstructure (Top view, phase-contrast micrographs; Side view, immunofluorescence micrographs; gray dashed lines, location of the porous basement membrane). Cultured cells were harvested and processed for scRNA-seq analysis by the 10x Genomics platform. Bars, 50 μm.

(B) A non-linear dimensionality reduction displayed in a UMAP that plots single cells from both culture formats. Cells from the Transwell culture have a homogeneous population (TW1), whereas the gut-on-a-chip culture demonstrated three heterogeneous subclusters (CHIP1, CHIP2, and CHIP3).

(C) A heatmap showing the top 15 genes differentially expressed in each cluster. The cluster colors illustrated in B are repeated. A complete list of selected genes is provided in Table S1.

was characterized. We offer mechanistic insight into a gut-on-a-chip culture on cytohistological development *in vitro* via single-cell transcriptomics and concomitant spatial visualization.

RESULTS

Single-cell transcriptomic characterization of culture-dependent epithelial heterogeneity

To characterize the epithelial heterogeneity depending on the culture format, Caco-2 cells were cultured in either a microfluidic gut-on-a-chip or a static Transwell for 5 days upon the formation of a confluent monolayer (Figure 1A). Although Caco-2 cells are typically cultured on Transwell inserts for 14-21 days post-confluency to induce differentiation, we performed a 5-day-long culture post-confluency to maintain identical culture conditions between two different culture formats. For instance, culture conditions such as culture medium, type of extracellular matrix (ECM) proteins, the concentration of ECM proteins for surface coating, passage number of Caco-2 cells, and seeding density of dissociated Caco-2 cells were synchronized. In a Transwell, cells adherent to the ECM-coated porous membrane formed a 2D monolayer with intact cell-cell junctions (Figure 1A, Transwell). On the contrary, Caco-2 epithelium grown in a gut-on-a-chip experienced physiological flow (50 μL/h, equivalent shear stress at 0.02 dyne/cm^2) and peristalsis-like rhythmical motions (10% in cell strain, 0.15 Hz in frequency), resulting in the regeneration of 3D epithelial layers as we previously discovered (Figure 1A, Gut-on-a-chip).[8–10] Next, we performed scRNA-seq followed

by the bioinformatic process including data quality control, variable gene selection, dimensionality reduction, and cell clustering using Seurat 3.[12] Differential gene expression from scRNA-seq resolved four clusters mapped on a Uni-form Mani-fold Approximation and Projection (UMAP)[13] (Figure 1B). Indeed, the physiologically dynamic culture in the gut-on-a-chip was the only source of variations in three clusters (CHIP1, CHIP2, and CHIP3), whereas the static Transwell culture resulted in a single isolated cluster (TW1). Interestingly, a heatmap that plots the top 15 genes most differentially expressed in each cluster (Table S1) involved the genes that regulate intestinal epithelial functions such as proliferation, regeneration, cell cycle, and differentiated intestinal functions such as molecular transport and drug metabolism (Figure 1C). For instance, CHIP1 cluster highlighted genes pertinent to the regulation of cell cycle and growth (*CDK1*,[14] *AREG*,[15] and *UBE2C*[16]) and mucosal barrier formation (*MUC13*).[17] CHIP2 showed a significant upregulation of genes associated with cell division and mitosis germane to 3D morphogenesis (*PTTG1*,[18] *CDC20*,[19] *CCNB1*,[20] *DDX21*,[21] and *MYC*[22]). In CHIP3, genes related to absorption and drug transport (*SLC2A3*, *SLC6A8*, *FXYD3*, *SLC11A2*, and *APOA4*)[23] were distinctively upregulated. TW1 cluster, in contrast, included upregulated genes related to cell mitosis (*HEPACAM2*),[24] mitogens (*FGB*, *FGG*, *FGA*),[25] and a colorectal cancer marker (*PHGR1*).[26] It is noted that the mitosis-related genes (*CDK1* and *UBE2C*) upregulated in CHIP1 were significantly downregulated in CHIP2, suggesting that a heterogeneous transcriptional process occurred in individual clusters of cells during the gut-on-a-chip culture. However, cell type-specific marker genes annotating enterocytes, goblet, enteroendocrine, enterochromaffin, tuft, Paneth, and microfold (M) cells[27] did not exclusively represent a particular cell cluster (Figure S1). Nonetheless, several genes representing each cell type were considerably upregulated in a particular cell cluster. For instance, CHIP3 showed higher expression of a couple of genes associated with Goblet cell characteristics compared to the other cell clusters. The Paneth cell-associated genes in CHIP1 and CHIP2 were also expressed more than those in CHIP3. This observation suggested that the CHIP clusters may possess spatial information within the formed 3D epithelial layers in a gut-on-a-chip.

Cluster-dependent spatial mapping in a gut-on-a-chip

Based on the primary clustering (Figure 1) and the expression of cell type marker genes (Figure S1), we retroactively verified if each cell cluster may encode spatial information in the 3D epithelial layer recreated in a gut-on-a-chip. We visually verified this hypothesis in the established histogenic structure in the gut-on-a-chip platform. Among the top 15 differentially expressed genes (Figure 1C), we chose *MUC13* and *CDK1* (CHIP1), *CCNB1* (CHIP2), and *SLC11A2* and *SLC6A8* (CHIP3), where the expression level in one cluster was significantly higher than the other clusters (Figure 2A and 2B). Next, we performed immunofluorescence confocal microscopic imaging by targeting the encoded proteins on 3D epithelial layers. The 3D rendered vertical cross-cut views (Figure 2C) revealed that the fluorescence signal of each marker illustrated the localized niche on the 3D epithelial layers recreated in the gut-on-a-chip (Figure 2D, top-down views focused on each designated location). The spatial signal of MUC13 and CDK1 (CHIP1) as well as CCNB1 (CHIP2) was predominantly localized in the middle-lower region near the basement membrane. On the contrary, multiple cells expressing SLC11A2 and SLC6A8 (CHIP3) were positioned in the upper-middle region of the 3D epithelial layer (Figure 2E). We also applied the previously annotated genes,[28] spatially zonated in the middle-upper (i.e., Top landmark genes) or the middle-lower region (i.e., Bottom landmark genes), to examine cluster-dependent spatial correlation. We found that CHIP3 showed higher expression of the Top landmark genes than the other clusters (Figure 2F, left), supporting the results of our spatial mapping. The expression of the Bottom landmark genes, however, was scattered across all CHIP clusters (Figure 2F, right).

Heterogeneous reprogramming in the developmental process and cell cycle

The spatial expression of the representative genes in each cluster (Figure 2) and the selected top 15 genes (Figure 1C) suggested that CHIP3 contains the most differentiated cell population, whereas CHIP1 and CHIP2 are dominated by proliferative cells that are transient to a differentiated stage. An unbiased pseudotemporal trajectory analysis additionally characterized this cellular and morphological reprogramming process to dissect the evolutionary transition of the Caco-2 cells and their subclusters depending on the culture format (Figure 3A). The merged 2D trajectory of all the clusters outlined a pseudotemporal propagation from the ancestral heredity (i.e., pseudotime is zero; dark blue) toward bifurcated branches (i.e., bright blue). When we determined TW1 cluster at the most ancestral position as a control (e.g., the left end branch), the cells in CHIP1 showed the most extensive spectrum of pseudotemporal distribution. On the contrary, the pseudotemporal points in CHIP2 and CHIP3 were found at the farthest positions from the ancestral TW1 cluster, suggesting that the cells cultured in the gut-on-a-chip were significantly evolved

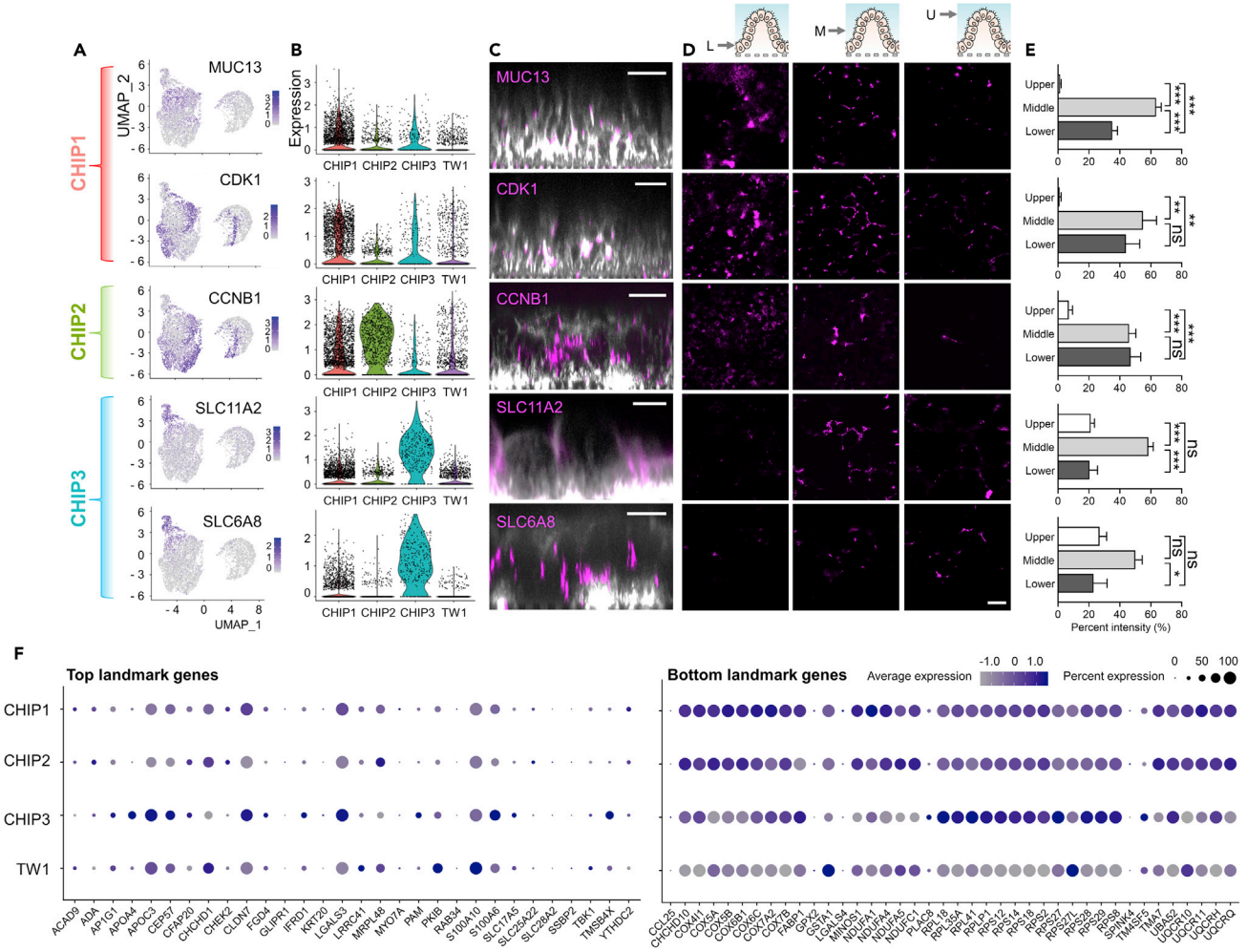

Figure 2. Spatial mapping of translated gene products after mechanodynamic cellular reprogramming

(A) The expression of 5 representative genes depicting each CHIP cluster is highlighted in the UMAP.

(B) Violin plots of scRNA-seq results corresponding to the selected genes in (A).

(C) Spatial localization of the selected gene products in 3D reconstruction views visualized by immunofluorescence confocal microscopy. Gray, F-actin; Magenta, corresponding proteins. Bars, 100 μm.

(D) Top-down confocal views of each corresponding marker expressed at different locations of the 3D epithelial layer. The focal plane of each image was designated in the schematic at lower (L), middle (M), or upper region (U). Bar, 50 μm.

(E) Quantifications of fluorescence signals in spatially resolved regions along the vertical direction. The upper, middle, and lower regions were determined by the location from the epithelial surface to the 1/3 location (Upper), from the 1/3 to the 2/3 location from the epithelial surface (middle), and from the 2/3 location to the bottom (Lower). N = 4. ns, not significant. *$p < 0.05$, **$p < 0.001$, ***$p < 0.0001$. Error bars, standard error of the mean.

(F) Dot plots that display the expression of the landmark genes relevant to villus zonation in each cluster. The average expression of the genes in each cluster is presented as a color scale and the proportion of cells expressing each gene is demonstrated as Percent expression (size of the dots). The landmark genes were adopted from a ref.[28] and listed in alphabetical order.

in the pseudotime configuration than in the static Transwell culture. This result shows a good agreement with the identified spatial information of the cell clusters verified in Figure 2.

The cell cycle analysis displayed on the UMAP (Figure 3B, left) reveals that the cells in CHIP1 and CHIP2 clusters showed higher populations of G2/M– and S-phases than the cells grown in the Transwell (Figure 3B, right). The cells in the TW1 cluster were composed of the most extensive G1 phase (68.18%) and the least G2/M (13.72%) and S phase (18.10%). Interestingly, the cell cycle frequency in the CHIP3 cluster (64.33, 15.24, and 20.43% of G1, G2M, and S phases, respectively) showed the highest similarity to the frequency in TW1, suggesting that the cellular dynamics of proliferation characterized by the cell

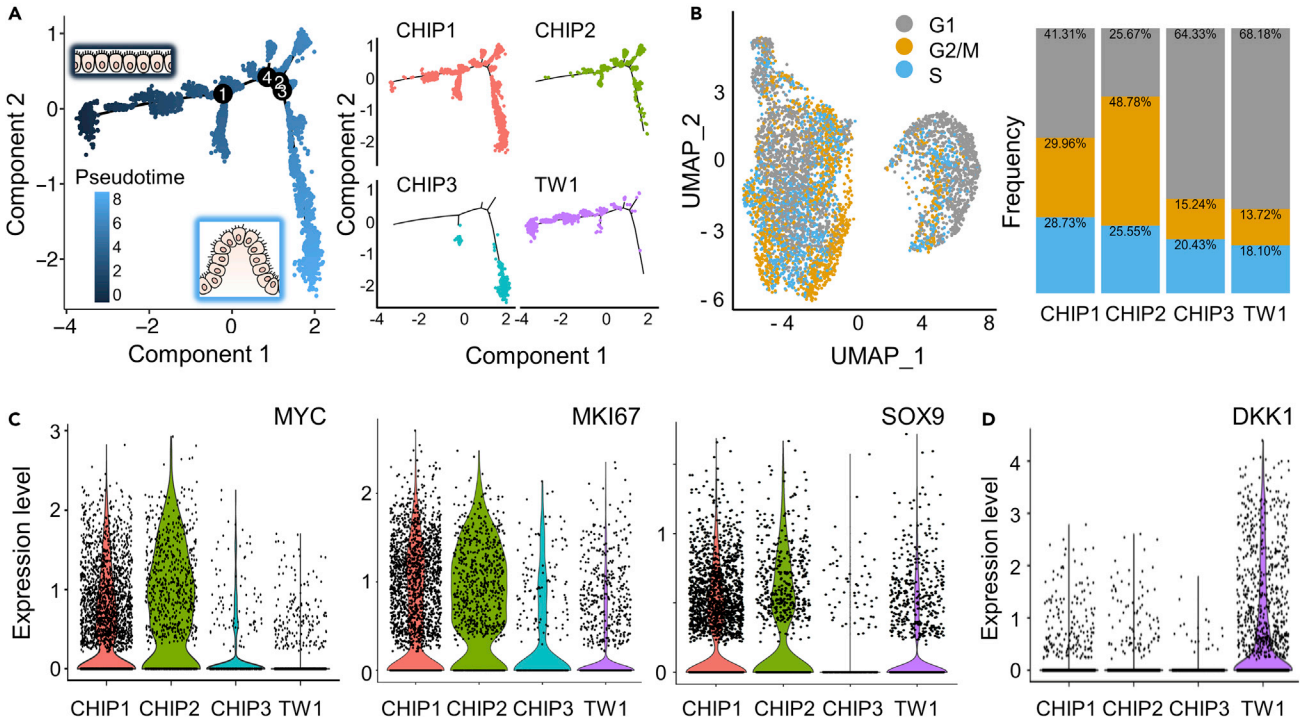

Figure 3. Heterogeneous cellular reprogramming in cell cycle and developmental process

(A) The collective pseudotemporal trajectory of single cells cultured in either a Transwell or a gut-on-a-chip (left) and individual pseudotemporal profiles with a cluster-dependent resolution (right). (Left) The cells in the TW1 cluster (dark blue) were assigned as the ancestral pseudotime, in which the cells in CHIP clusters were widely distributed in branched pseudotemporal trajectories (lighter blue), indicating the heterogeneous evolutionary reprogramming. The branching points are labeled in circled numbers. The inset schematics illustrate the shape of a cell layer in TW1 (left top; 2D) or CHIP (right bottom; 3D). (Right) The pseudotemporal distribution of individual clusters that have the paired color coordination with Figure 1B.

(B) Distribution of individual single cells that show distinct cell cycles in G1 (gray), G2/M (orange), or S phase (sky blue) plotted on the UMAP (left) and the frequency of single cells in each cluster.

(C and D) Violin plots that represent the significant upregulation of (C) *MYC*, *MKI67*, and *SOX9* in CHIP1 and CHIP2 clusters and (D) the elevated expression of *DKK1* in the TW1 cluster.

cycle analysis is minimal in both clusters. Regardless of the similar cell cycle patterns, it is noted that the morphological and spatial transcriptomic signatures of the Caco-2 cells cultured in the gut-on-a-chip were distinct from the ones prepared in the Transwell, indicating that mechanodynamic on-chip cultures dramatically induce cellular reprogramming of Caco-2 cells in shapes and functions with greater *in vivo* relevance than static Transwell cultures. The profile of mitochondrial genes (%MT) also showed a good agreement with the cell cycle analysis (Figure S2).[29,30] Indeed, both CHIP1 and CHIP2 clusters showed a significantly elevated population of cells (<75%) in G2/M or S phase than CHIP3 (Figure 3B), suggesting that the dynamics of cell cycle and mitosis was perturbed to be heterogeneous when cells were cultured in the mechanodynamic gut-on-a-chip device.

It is notable that the heterogeneity of transcriptomic signature regarding cell proliferation was also represented in the expression of genes encoding proto-oncogenic transcription factor (*MYC*),[22] proliferation (*MKI67*),[31] and stem cells (*SOX9*),[32] in which both CHIP1 and CHIP2 clusters showed the remarkable elevation of those genes than CHIP3 and TW1 clusters (Figure 3C). Interestingly, although the CHIP3 cluster showed similar patterns in cell cycle and proliferation with TW1, a representative Wnt-antagonizing gene, Dickkopf-related protein 1 (*DKK1*),[33] that is critical for intestinal morphogenesis in a gut-on-a-chip[10,11] was minimally expressed in all the CHIP clusters, whereas TW1 was a dominant cluster that shows considerable upregulation of *DKK1* (Figure 3D). This result shows good accordance with our previous finding that the removal of basolaterally secreted DKK1 molecules in a gut-on-a-chip leads to 3D epithelial morphogenesis, whereas a static Transwell culture that accumulates extracellular DKK-1 considerably restricts the morphogenic process regardless of the culture period.[9,10] The transcriptomic heterogeneity of epithelial growth dynamics was also verified by a couple of gene ontology (GO) snapshots on the

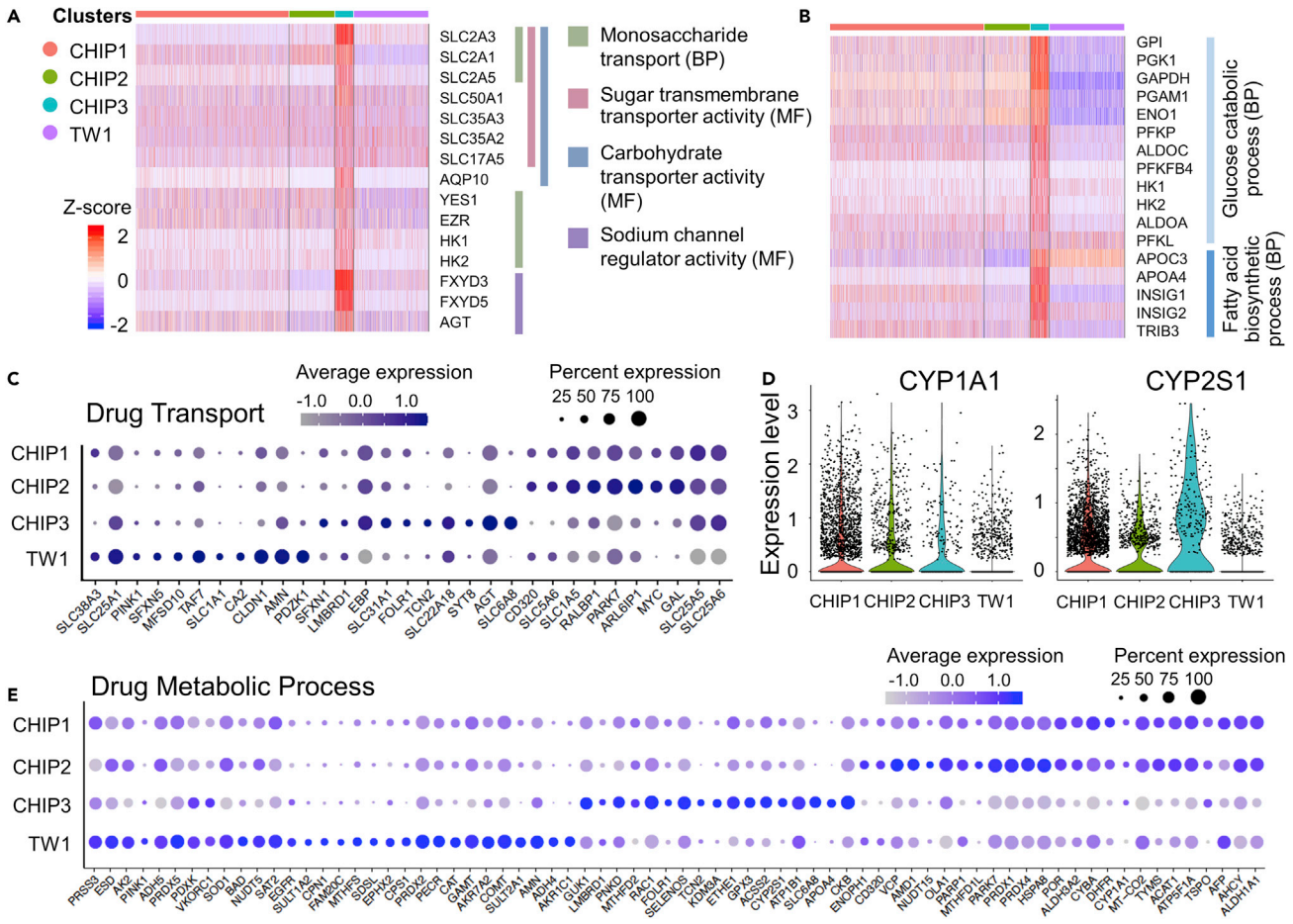

Figure 4. Transcriptomic perturbation of the genes associated with intestinal epithelial functions and drug metabolism

(A) A heatmap that summarizes the expression of the genes associated with the GO terms of monosaccharide transport (BP), sugar transmembrane transporter activity (MF), carbohydrate transporter activity (MF), and sodium channel regulator activity (MF). BP, biological process, MF, molecular function. Vertical color bars indicate the genes corresponding to the associated BP or MF.

(B) A heatmap that profiles the expression of genes involved in the GO terms of glucose catabolic process (BP) and fatty acid biosynthetic process (BP).

(C) A dot plot that displays the reprogrammed single-cell transcriptomes pertinent to drug transport.

(D) Violin plots that highlight the elevated expression of *CYP1A1* and *CYP2S1* in CHIP clusters compared to TW1.

(E) A dot plot that visualizes the perturbed expression of genes regulating the drug-metabolizing process.

heterogeneous signaling perturbations of Wnt (Figure S3), Notch (Figure S4), and bone morphogenetic protein (BMP) pathways (Figure S5). The genes regulating planar cell polarity showed the least expression in CHIP3, while the most upregulation was confirmed in CHIP2 that also support the spatial information that the CHIP clusters possess (Figure S6). It is noted that a considerable number of genes displayed in these cell signaling pathways were upregulated in CHIP clusters than TW1.

Transcriptomic perturbation in epithelial functions and drug metabolism

Next, we examined the heterogeneity of transcriptomes in each cluster related to fundamental epithelial functions such as nutrient absorption and transport, biosynthetic process, and drug metabolism. We found that the expression of genes pertinent to monosaccharide transport, sugar transmembrane transporter activity, carbohydrate transporter activity, and sodium channel regulator activity (Figure 4A), glucose catabolic process, and fatty acid biosynthesis (Figure 4B) were all significantly higher in CHIP3 than the other clusters. This result is well matched with the spatial information that the cells in CHIP3 are located in the mid-upper region of the 3D epithelial layer because these transport activities, catabolism, and fatty acid biosynthesis are regulated at the mucosal surface mainly by enterocytes.[34] The gene set enrichment analysis (GSEA) that compares the most significant 33 GO terms also verified that the gene sets associated with

intestinal molecular transport (e.g., monosaccharide transport, sugar transmembrane transporter activity, sodium channel regulator activity, carbohydrate transporter activity, and other biosynthetic activity) were upregulated in CHIP3 compared to both CHIP1 and CHIP2 clusters (Figure S7A). This result also shows a strong correlation with the results provided in Figure 4A. When the most significant 33 GO terms were compared between TW1 and all the CHIP clusters (Figure S7B), we found that the gene set associated with glucose catabolic process significantly upregulated in the CHIP clusters, which showed good agreement with the results in Figure 4B as the genes germane to glucose catabolic process (BP) were substantially downregulated in the TW cluster. We additionally mapped an overall transcriptome profile of transporters targeting water, vitamin, bile salt, lipid, organic solute, inorganic solute, amino acid, nucleotide, metal ion, and sugar, confirming heterogeneous reprogrammed features of Caco-2 cells cultured in the gut-on-a-chip (Figure S8). Some of the genes of the SLC26 family (ion exchanger) and SLC9 family (Na^+/H^+ exchanger or scaffold) that are often characterized in Caco-2 models showed distinctively higher expressions in either CHIP3 or TW1 cluster. For instance, *SLC26A2*, *SLC26A6*, and *SLC9A2* showed the highest expressions in CHIP3, and *SLC26A3* and *SLC9A3R1* showed higher expressions in TW1. Notably, approximately two-thirds of the genes linked to the GO Drug Transport process were considerably upregulated in CHIP clusters (e.g., *SLC1A5*, *RALBP1*, *GAL*, *TCN2*, *SYT8*, and *SLC25A5*), while the genes highlighted in TW1 cluster represented conserved epithelial functions such as glutamate transport (*SLC1A1*)[35] or acid-base homeostasis (*CA2*; Figure 4C).[36] Moreover, the gut-on-a-chip culture elicited Caco-2 cells to show reprogrammed drug-metabolizing characteristics,[9] where the heterogeneous population of single cells harvested from the gut-on-a-chip showed elevated expression of genes encoding Phase I (*CYP1A1*, *CYP2S1*, and *ALDH1A1*; Figures 4D and S9) and Phase II (*AHCY*) enzymes as well as a Phase III transporter (*SLC6A8*; Figure 4E).[37]

Transcriptomic perturbation of cancer-associated genes

Notably, the Caco-2 cells that underwent the on-chip mechanodynamic cultures showed a significant transcriptomic perturbation of genes germane to oncogenic or tumor-suppressive functions. Using the Cancer Gene Census database,[38] we selected the genes associated with colorectal cancer, then regrouped them into oncogenes and tumor suppressor genes. The oncogene group revealed a decreased expression in all the CHIP clusters compared to the TW1 cluster (Figure 5A). On the contrary, the tumor-suppressor genes showed substantial upregulations in all the CHIP clusters, especially in CHIP3, compared to TW1 (Figure 5B). We confirmed that colon-specific cancer stem cell markers including *PHGR1*,[26] *PROM1* (encoding CD133),[39] and *DPP4*[40] also showed a significant reduction of expressions (Figure 5C), suggesting that a mechanodynamic gut-on-a-chip culture of Caco-2 cells drives a post-mitotic reprogramming of cancer-associated phenotypes along with other essential epithelial functions.

DISCUSSION

In this study, we used the Transwell format as a static control culture, given that Caco-2 cells cultured on a Transwell is one of the most popular culture setups to establish intestinal mucosal barrier and test intestinal permeability.[5,6] While Caco-2 cells have been predominantly cultured and utilized in static Transwell cultures, *in vivo*-relevant phenotypic heterogeneity has only been demonstrated in mechanodynamic gut-on-a-chip cultures.[9] The investigation of single-cell transcriptomics in the current study supports the previous findings of cellular reprogramming by showing spatially localized heterogeneous cell populations, pseudotemporal development, physiological functions, and reversion of cancer-related transcriptomes.

In the current study, we observed that the identified cell clusters did not exclusively represent specific cell types. Possible explanations are as follows. First, the cytodifferentiation may not be sufficiently induced within a 5-day-long gut-on-a-chip culture. The analysis of actual temporal transcriptomic dynamics as a function of the culture period (rather than the pseudotemporal dynamics as we performed in this study) may be a possible direction to provide greater biological insights in the future. Second, cell type annotation based on single-cell transcriptomes is still a developing technology in the bioinformatics research field[41] and is in part subjective because the gene expression is in continuum and not binary.[42–44] Finally, some transcriptomes of Caco-2 cells may be unresponsive to biomechanical and physiological stimulations during the on-chip cultures.

The spatial mapping of the selected genes in each CHIP cluster suggested that the clusters derived from a gut-on-a-chip culture may undergo distinct spatial organization of proliferative and differentiated cells along the migration axis from the basement membrane toward the upper region of a mucosal surface,

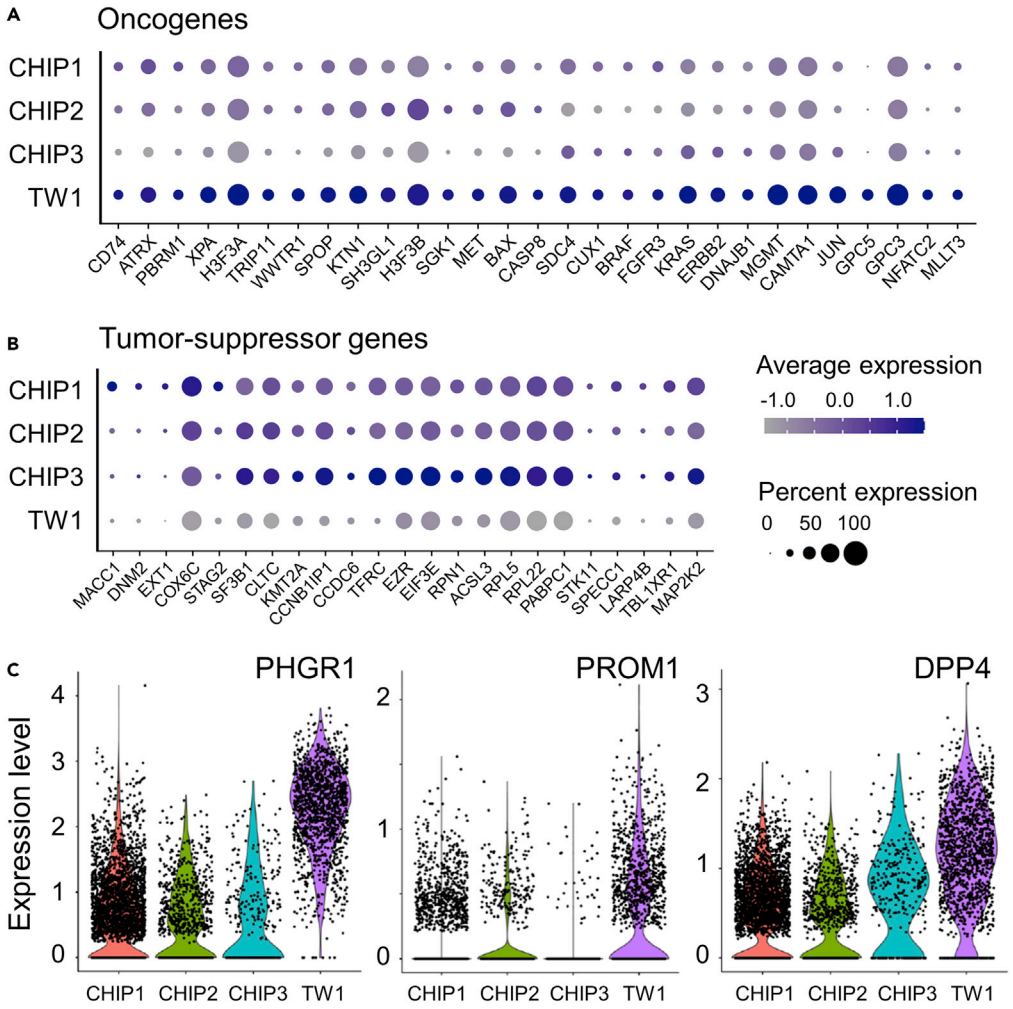

Figure 5. Reprogrammed transcriptomic feature of cancer inheritance on Caco-2 cells

(A) A dot plot that summarizes the reduced expression of transcriptomic signature of oncogenes in the mechanodynamic gut-on-a-chip cultures than the static Transwell cultures.

(B) A dot plot that displays the enhanced expression of tumor-suppressor genes in the mechanodynamic gut-on-a-chip cultures than the static Transwell cultures.

(C) Violin plots that visualize the expression of representative markers of colon cancer stem cells, *PHGR1*, *PROM1*, and *DPP4* between clusters.

reminiscent of the crypt-villus axis *in vivo*. We previously reported a similar epithelial behavior using a gut-on-a-chip, where EdU-positive proliferative cells migrated from the basal region near the basement membrane to the epithelial tip.[9] The result was also, in part, correlated with the physiological functions of genes that we highlighted in this analysis. For instance, *CDK1* represented in the CHIP1 cluster showed higher expression in the proliferating basal area, which is involved in the cell cycle and apoptotic regulations.[45] CHIP2 representing *CCNB1* that encodes cyclin B1 regulates the transition process from G2 to M phase in the cell cycle.[46] Therefore, the localized expression of *CCNB1* in the middle-lower region of the 3D epithelial layer agrees with its known roles and spatial location *in vivo*. The selected genes for CHIP3, *SLC6A8*, and *SLC11A2* are a Na^+ Cl^- dependent creatine transporter and a metal transporter,[47,48] respectively. These transporters are known to be expressed predominantly in the intestinal villi rather than the crypt *in vivo*, which was visually confirmed in our study. It is noted that the *in vitro* 3D morphogenesis that spontaneously occurs in a gut-on-a-chip[10] offers a compelling spatial mapping with visual modalities of the selected genes pertinent to transcriptomic perturbations. When we analyzed the expression of villus zonation genes,[28] however, the Bottom landmark genes did not show significantly higher expressions in CHIP1 and CHIP2. We suppose this is because the 3D Caco-2 epithelium cultured in a gut-on-a-chip

contains an actively proliferating cell population (i.e., CHIP1 and CHIP2), whereas the zonation marker genes were distinguished based on mouse villi that are composed of fully differentiated cells. Further visual characterization of such zonation markers by integrating single-cell spatial transcriptomics at molecular and cellular levels will be of great interest in future studies.

The genes regulating planar cellular polarity showed the least expression in the CHIP3 cluster, while the most upregulation was confirmed in the CHIP2 cluster. This result supports our observation because cell polarity is thought to be reduced at or near the villus tip *in vivo* because of shedding-out cells at the tip of the intestinal epithelium.[49] It is noted that the cells in CHIP3 are located more in the upper region of 3D epithelium formed in a gut-on-a-chip.

We found significantly increased expression of oncogenes in TW1 compared to CHIP clusters, whereas *MYC* showed lower expression in TW1. Although MYC family proteins are often considered proto-oncogenes, they are also the transcription factors that regulate the expression of multiple pro-proliferative stem cells while inhibiting the differentiation of cells in normal intestinal regeneration.[22] Furthermore, not all cancer cells show overexpression of the *MYC* gene, whereas low *MYC*-expressing cancer cells often have a higher metastatic capability.[50] Notably, we applied the same culture medium containing a high-content serum (e.g., 20% FBS, v/v) in both cultures, suggesting that the culture medium is not a factor that orchestrates the distinctive expression of *MYC* between TW1 and CHIP clusters. Importantly, when Caco-2 cells form a 3D epithelial microarchitecture, proliferative cells in the basal area spontaneously migrate upward to the epithelial tip, then are shed out (Kim and Ingber, *Integr. Biol.*, 2013). On the contrary, Caco-2 cells grown on a Transwell insert do not show this histogenic behavior because they only have a 2D monolayer regardless of culture medium or serum content. Upon this morphological difference, the dynamic turnover of Caco-2 cells proliferative and migrating in the basal layer may contribute to showing the elevated level of *MYC* expression in the gut-on-a-chip, representing CHIP1 and CHIP2 in the current study. The mechanodynamic microenvironment established in a gut-on-a-chip may be a prerequisite for perturbing transcriptomic profiles of Caco-2 cells, including *MYC*, *MKI67*, *SOX9*, and *DKK1* which are critical to inducing the intestinal developmental process.

Our study also provides intriguing insights into various transporter genes with cluster-dependent spatial characteristics. The expression of *SLC26A3* (chloride anion exchanger) in the CHIP clusters was relatively lower than that in the TW cluster (Figure S8, "Inorganic solute"). Among the CHIP clusters, its expression was the least in CHIP2, where CHIP1 and CHIP3 showed comparable expression levels with each other. One possibility is that CHIP2 has the highest population of proliferating cells. Thus, less population of differentiated cells is anticipated in this cluster. We found that the expression of *SLC9A2* (sodium-hydrogen exchanger 2 or NHE2; Figure S8, "Metal ion") is the highest in CHIP3. It is noted that the spatial expression of *SLC9A2* is known to be species-dependent. For instance, NHE2 is expressed in the crypts in mice or on the whole surface of the villus or upper half of the colonic crypt in rabbits.[51,52] Yet, no published report shows the expression of NHE2 in the human intestine. At the mRNA level, however, NHE2 is expressed throughout the vertical axis of the crypt in the human colon.[53] Therefore, it may be necessary to perform comparative analyses between the *in vitro* epithelium formed in a gut-on-a-chip and actual human intestinal tissue. We also found that the epithelial sodium channel (ENaC, *SCNN1A*) shows the highest expression in CHIP3 (Figure S8, "Metal ion"), which aligns well with the existing knowledge that ENaC is expressed on the surface of the intestinal epithelium.

Our study presents several disseminating impacts. First, the legitimacy and validity of Caco-2 cells in pharmaceutical applications may be repurposed when the cells undergo mechanodynamic stimulations and 3D morphogenesis in a gut-on-a-chip. Since Caco-2 cells have been used in pharmaceutical and biomedical studies over the past couple of decades, it may be an attractive option to induce directional reprogramming of Caco-2 cells and enhance the utility for defined applications. Second, this study did not involve cellular and molecular engineering (e.g., CRISPR-based genome engineering) nor surrounding cellular components (e.g., stromal cells, immune cells, or microbiome) that can alter cellular plasticity at various disease milieus. Hereby, we confirmed that a mechanodynamic gut-on-a-chip culture is necessary and sufficient for Caco-2 cells to be reprogrammed to elicit *in vivo*-relevant heterogeneous physiological functions. Finally, the reversion of cancerous characteristics to the normal by simply culturing cells in a gut-on-a-chip suggests a novel avenue of mechanistic cancer studies. Our results suggest that conventional static *in vitro* cultures, from immortalized cell lines to patient-derived organoid cultures, may need to be

significantly improved by adapting mechanodynamic on-chip cultures because *in vitro* static cultures neither restore the *in vivo*-relevant original phenotypic characteristics nor recapitulate physiological and pathological responses. Indeed, the human gut-on-a-chip may suggest an alternative culture platform to accurately manipulate the tissue microenvironment to investigate cellular developmental process, molecular interactions in a spatiotemporal landscape, selected stimulation with a directional configuration (e.g., apical vs. basolateral), and time-resolved multi-modal assessments.

In summary, we elucidated that a mechanodynamic culture in a human gut-on-a-chip enhances intestinal physiological functions of Caco-2 cells, where notably, the chemical and nutritional environment was identical to the static Transwell cultures. We verified that Caco-2 cells spontaneously undergo reprogramming of transcriptomic signature, pseudotemporal trajectory, spatial reorganization of epithelium in a basal-mucosal axis, restoration of genes associated with normal intestinal functions, and reversion from cancerous to normal transcriptomic patterns when cultured in a mechanodynamic gut-on-a-chip. We envision that our proof-of-principle study will disseminate a practical and implementable approach to be applicable to other tissue-derived or iPSC-derived primary cells under a defined biomechanical, chemical, and physiological condition.

Limitations of the study

The current study employed an immortalized Caco-2 adenocarcinoma line to verify the impact of mechanodynamic gut-on-a-chip cultures on transcriptomic perturbation and reprogramming. Thus, the formed 3D epithelium may not sufficiently reflect the characteristics of the normal intestine. Also, since the on-chip cultures begin with a monolayer of Caco-2 cells, there are neither crypt-like spatial loci nor clear villus compartmentalization even after the cells form 3D epithelial microarchitecture. This circumstance may cause "piled-up" cells near the basal area; nonetheless, the middle-upper region of the 3D epithelial layers reproducibly shows a single monolayer of epithelial cells as a landmark morphology of intestinal epithelium *in vivo*. As discussed previously, our current study only conveys intestinal epithelium, by which the impact of surrounding cells such as stromal cells, immune cells, or gut microbiota may need to be additionally investigated. Also, the single-cell transcriptomic profile in this study does not provide a complete set of cell type-specific clusters. This circumstance may result in limited expressions of some prospective genes with a lack of cluster-dependent characteristic accordance. For instance, we found that the distribution of drug transporters in our current study does not thoroughly fit with the protein distribution in the normal human intestine, suggesting that the expression patterns of individual genes do not always match the spatial information we identified in the CHIP clusters. Hence, additional single-cell transcriptomic studies using human primary intestinal epithelial cells cultured in the same gut-on-a-chip device may be required to understand if this discrepancy may be driven by the innate nature of the cancer cell line that conveys multiple truncated mutations.[54,55]

STAR★METHODS

Detailed methods are provided in the online version of this paper and include the following:

- KEY RESOURCES TABLE
- RESOURCE AVAILABILITY
  - Lead contact
  - Materials availability
  - Data and code availability
- EXPERIMENTAL MODEL AND SUBJECT DETAILS
- METHOD DETAILS
  - Microfabrication of a gut-on-a-chip
  - Culture of Caco-2 cells in a transwell and a gut-on-a-chip
  - Sample preparation for scRNA-seq analysis
  - Image analysis
  - Mapping and aggregation
  - Quality control and single-cell transcriptomic analyses
  - Pseudotemporal trajectory analysis
  - Identification of marker genes and gene set enrichment analysis
  - Correction of batch effect, data normalization, and concatenation
- QUANTIFICATION AND STATISTICAL ANALYSIS

SUPPLEMENTAL INFORMATION

Supplemental information can be found online at https://doi.org/10.1016/j.isci.2022.105521.

ACKNOWLEDGMENTS

This work was supported in part by the National Cancer Institute of the National Institutes of Health (NIH/NCI) F99/K00 Predoctoral to Postdoctoral Transition Award (K00CA245801 to W.S.), Asan Foundation Biomedical Science Scholarship (W.S.), Mogam Science Scholarship (W.S.), the National Institute of General Medical Sciences (NIH/NIGMS) Maximizing Investigators' Research Award (MIRA) (R35 GM133658 to S.S.Y.), NIH/NCI Innovative Molecular Analysis Technologies (IMAT) program (R21CA236690 to H.J.K.), and the Leona M. and Harry B. Helmsley Charitable Trust (H.J.K.).

AUTHOR CONTRIBUTIONS

W.S. and H.J.K. conceived and designed the study and performed experiments. W.S., Z.S., S.S.Y., and H.J.K. analyzed the data and wrote the article.

DECLARATION OF INTERESTS

The authors declare no conflict of interest.

INCLUSION AND DIVERSITY

We support inclusive, diverse, and equitable conduct of research.

Received: November 28, 2021
Revised: September 18, 2022
Accepted: November 3, 2022
Published: December 22, 2022

REFERENCES

1. Meunier, V., Bourrié, M., Berger, Y., and Fabre, G. (1995). The human intestinal epithelial cell line Caco-2; pharmacological and pharmacokinetic applications. Cell Biol. Toxicol. *11*, 187–194. https://doi.org/10.1007/BF00756522.

2. Iftikhar, M., Iftikhar, A., Zhang, H., Gong, L., and Wang, J. (2020). Transport, metabolism and remedial potential of functional food extracts (FFEs) in Caco-2 cells monolayer: a review. Food Res. Int. *136*, 109240. https://doi.org/10.1016/j.foodres.2020.109240.

3. Jarc, T., Novak, M., Hevir, N., Rižner, T.L., Kreft, M.E., and Kristan, K. (2019). Demonstrating suitability of the Caco-2 cell model for BCS-based biowaiver according to the recent FDA and ICH harmonised guidelines. J. Pharm. Pharmacol. *71*, 1231–1242. https://doi.org/10.1111/jphp.13111.

4. Sääf, A.M., Halbleib, J.M., Chen, X., Yuen, S.T., Leung, S.Y., Nelson, W.J., et al. (2007). Parallels between global transcriptional programs of polarizing Caco-2 intestinal epithelial cells in vitro and gene expression programs in normal colon and colon cancer. Mol. Biol. Cell *18*, 4245–4260. https://doi.org/10.1091/mbc.e07-04-0309.

5. Natoli, M., Leoni, B.D., D'Agnano, I., Zucco, F., and Felsani, A. (2012). Good Caco-2 cell culture practices. Toxicol. Vitro *26*, 1243–1246. https://doi.org/10.1016/j.tiv.2012.03.009.

6. Sambuy, Y., De Angelis, I., Ranaldi, G., Scarino, M.L., Stammati, A., and Zucco, F. (2005). The Caco-2 cell line as a model of the intestinal barrier: influence of cell and culture-related factors on Caco-2 cell functional characteristics. Cell Biol. Toxicol. *21*, 1–26. https://doi.org/10.1007/s10565-005-0085-6.

7. Verhoeckx, K., Cotter, P., López-Expósito, I., Kleiveland, C., Lea, T., Mackie, A., Requena, T., Swiatecka, D., and Wichers, H. (2015). The Impact of Food Bioactives on Health: In Vitro and Ex Vivo Models (Springer).

8. Kim, H.J., Huh, D., Hamilton, G., and Ingber, D.E. (2012). Human gut-on-a-chip inhabited by microbial flora that experiences intestinal peristalsis-like motions and flow. Lab Chip *12*, 2165–2174. https://doi.org/10.1039/c2lc40074j.

9. Kim, H.J., and Ingber, D.E. (2013). Gut-on-a-Chip microenvironment induces human intestinal cells to undergo villus differentiation. Integr. Biol. *5*, 1130–1140. https://doi.org/10.1039/c3ib40126j.

10. Shin, W., Hinojosa, C.D., Ingber, D.E., and Kim, H.J. (2019). Human intestinal morphogenesis controlled by transepithelial morphogen gradient and flow-dependent physical cues in a microengineered gut-on-a-chip. iScience *15*, 391–406. https://doi.org/10.1016/j.isci.2019.04.037.

11. Shin, W., and Kim, H.J. (2022). 3D in vitro morphogenesis of human intestinal epithelium in a gut-on-a-chip or a hybrid chip with a cell culture insert. Nat. Protoc. *17*, 910–939. https://doi.org/10.1038/s41596-021-00674-3.

12. Stuart, T., Butler, A., Hoffman, P., Hafemeister, C., Papalexi, E., Mauck, W.M., 3rd, Hao, Y., Stoeckius, M., Smibert, P., and Satija, R. (2019). Comprehensive integration of single-cell data. Cell *177*, 1888–1902.e21. https://doi.org/10.1016/j.cell.2019.05.031.

13. Becht, E., McInnes, L., Healy, J., Dutertre, C.A., Kwok, I.W.H., Ng, L.G., Ginhoux, F., and Newell, E.W. (2018). Dimensionality reduction for visualizing single-cell data using UMAP. Nat. Biotechnol. *37*, 38–44. https://doi.org/10.1038/nbt.4314.

14. McCusker, D., Denison, C., Anderson, S., Egelhofer, T.A., Yates, J.R., 3rd, Gygi, S.P., and Kellogg, D.R. (2007). Cdk1 coordinates cell-surface growth with the cell cycle. Nat. Cell Biol. *9*, 506–515. https://doi.org/10.1038/ncb1568.

15. Shao, J., and Sheng, H. (2010). Amphiregulin promotes intestinal epithelial regeneration: roles of intestinal subepithelial myofibroblasts. Endocrinology *151*, 3728–3737. https://doi.org/10.1210/en.2010-0319.

16. Bajaj, S., Alam, S.K., Roy, K.S., Datta, A., Nath, S., and Roychoudhury, S. (2016). E2 ubiquitin-conjugating enzyme, UBE2C gene, is reciprocally regulated by wild-type and gain-of-function mutant p53. J. Biol. Chem. *291*, 14231–14247. https://doi.org/10.1074/jbc.M116.731398.

17. Sheng, Y.H., Lourie, R., Lindén, S.K., Jeffery, P.L., Roche, D., Tran, T.V., Png, C.W., Waterhouse, N., Sutton, P., Florin, T.H.J., and McGuckin, M.A. (2011). The MUC13 cell-surface mucin protects against intestinal inflammation by inhibiting epithelial cell apoptosis. Gut *60*, 1661–1670. https://doi.org/10.1136/gut.2011.239194.

18. Ishitsuka, Y., Kawachi, Y., Taguchi, S., Maruyama, H., Fujisawa, Y., Furuta, J., Nakamura, Y., and Otsuka, F. (2012). Pituitary tumor-transforming gene 1 enhances proliferation and suppresses early differentiation of keratinocytes. J. Invest. Dermatol. *132*, 1775–1784. https://doi.org/10.1038/jid.2012.74.

19. Yang, W., Wightman, R., and Meyerowitz, E.M. (2017). Cell cycle control by nuclear sequestration of CDC20 and CDH1 mRNA in plant stem cells. Mol. Cell *68*, 1108–1119.e3. https://doi.org/10.1016/j.molcel.2017.11.008.

20. Whitfield, M.L., Sherlock, G., Saldanha, A.J., Murray, J.I., Ball, C.A., Alexander, K.E., Matese, J.C., Perou, C.M., Hurt, M.M., Brown, P.O., and Botstein, D. (2002). Identification of genes periodically expressed in the human cell cycle and their expression in tumors. Mol. Biol. Cell *13*, 1977–2000. https://doi.org/10.1091/mbc.02-02-0030.

21. Sergeeva, O., and Zatsepin, T. (2021). RNA helicases as shadow modulators of cell cycle progression. Int. J. Mol. Sci. *22*, 2984. https://doi.org/10.3390/ijms22062984.

22. Bettess, M.D., Dubois, N., Murphy, M.J., Dubey, C., Roger, C., Robine, S., et al. (2005). c-Myc is required for the formation of intestinal crypts but dispensable for homeostasis of the adult intestinal epithelium. Mol. Cell Biol. *25*, 7868–7878. https://doi.org/10.1128/MCB.25.17.7868-7878.2005.

23. Ye, A.Y., Liu, Q.-R., Li, C.-Y., Zhao, M., and Qu, H. (2014). Human transporter database: comprehensive knowledge and discovery tools in the human transporter genes. PLoS One *9*, e88883. https://doi.org/10.1371/journal.pone.0088883.

24. Asou, H., Matsui, H., Ozaki, Y., Nagamachi, A., Nakamura, M., Aki, D., and Inaba, T. (2009). Identification of a common microdeletion cluster in 7q21.3 subband among patients with myeloid leukemia and myelodysplastic syndrome. Biochem. Biophys. Res. Commun. *383*, 245–251. https://doi.org/10.1016/j.bbrc.2009.04.004.

25. Sörensen, I., Susnik, N., Inhester, T., Degen, J.L., Melk, A., Haller, H., et al. (2011). Fibrinogen, acting as a mitogen for tubulointerstitial fibroblasts, promotes renal fibrosis. Kidney Int. *80*, 1035–1044. https://doi.org/10.1038/ki.2011.214.

26. Oltedal, S., Skaland, I., Maple-Grødem, J., Tjensvoll, K., Janssen, E.A.M., Gilje, B., Smaaland, R., Heikkilä, R., and Nordgård, O. (2018). Expression profiling and intracellular localization studies of the novel Proline-Histidine-and Glycine-rich protein 1 suggest an essential role in gastro-intestinal epithelium and a potential clinical application in colorectal cancer diagnostics. BMC Gastroenterol. *18*, 26. https://doi.org/10.1186/s12876-018-0752-8.

27. Franzén, O., Gan, L.M., and Björkegren, J.L.M. (2019). PanglaoDB: a web server for exploration of mouse and human single-cell RNA sequencing data. Database *2019*, baz046. https://doi.org/10.1093/database/baz046.

28. Moor, A.E., Harnik, Y., Ben-Moshe, S., Massasa, E.E., Rozenberg, M., Eilam, R., Bahar Halpern, K., and Itzkovitz, S. (2018). Spatial reconstruction of single enterocytes uncovers broad zonation along the intestinal villus Axis. Cell *175*, 1156–1167.e15. https://doi.org/10.1016/j.cell.2018.08.063.

29. Márquez-Jurado, S., Díaz-Colunga, J., das Neves, R.P., Martinez-Lorente, A., Almazán, F., Guantes, R., and Iborra, F.J. (2018). Mitochondrial levels determine variability in cell death by modulating apoptotic gene expression. Nat. Commun. *9*, 389. https://doi.org/10.1038/s41467-017-02787-4.

30. Xiong, W., Jiao, Y., Huang, W., Ma, M., Yu, M., Cui, Q., and Tan, D. (2012). Regulation of the cell cycle via mitochondrial gene expression and energy metabolism in HeLa cells. Acta Biochim. Biophys. Sin. *44*, 347–358. https://doi.org/10.1093/abbs/gms006.

31. Scholzen, T., and Gerdes, J. (2000). The Ki-67 protein: from the known and the unknown. J. Cell. Physiol. *182*, 311–322. https://doi.org/10.1002/(SICI)1097-4652(200003)182:3<311::AID-JCP1>3.0.CO;2-9.

32. Jo, A., Denduluri, S., Zhang, B., Wang, Z., Yin, L., Yan, Z., Kang, R., Shi, L.L., Mok, J., Lee, M.J., and Haydon, R.C. (2014). The versatile functions of Sox9 in development, stem cells, and human diseases. Genes Dis. *1*, 149–161. https://doi.org/10.1016/j.gendis.2014.09.004.

33. Niida, A., Hiroko, T., Kasai, M., Furukawa, Y., Nakamura, Y., Suzuki, Y., Sugano, S., and Akiyama, T. (2004). DKK1, a negative regulator of Wnt signaling, is a target of the beta-catenin/TCF pathway. Oncogene *23*, 8520–8526. https://doi.org/10.1038/sj.onc.1207892.

34. Kiela, P.R., and Ghishan, F.K. (2016). Physiology of intestinal absorption and secretion. Best Pract. Res. Clin. Gastroenterol. *30*, 145–159. https://doi.org/10.1016/j.bpg.2016.02.007.

35. Arnold, P.D., Sicard, T., Burroughs, E., Richter, M.A., and Kennedy, J.L. (2006). Glutamate transporter gene SLC1A1 associated with obsessive-compulsive disorder. Arch. Gen. Psychiatry *63*, 769–776. https://doi.org/10.1001/archpsyc.63.7.769.

36. Zheng, J., Avvaru, B.S., Tu, C., McKenna, R., and Silverman, D.N. (2008). Role of hydrophilic residues in proton transfer during catalysis by human carbonic anhydrase II. Biochemistry *47*, 12028–12036. https://doi.org/10.1021/bi801473w.

37. Xu, C., Li, C.Y.T., and Kong, A.N.T. (2005). Induction of phase I, II and III drug metabolism/transport by xenobiotics. Arch Pharm. Res. *28*, 249–268. https://doi.org/10.1007/BF02977789.

38. Sondka, Z., Bamford, S., Cole, C.G., Ward, S.A., Dunham, I., and Forbes, S.A. (2018). The COSMIC Cancer Gene Census: describing genetic dysfunction across all human cancers. Nat. Rev. Cancer *18*, 696–705. https://doi.org/10.1038/s41568-018-0060-1.

39. Ren, F., Sheng, W.-Q., and Du, X. (2013). CD133: a cancer stem cells marker, is used in colorectal cancers. World J. Gastroenterol. *19*, 2603–2611. https://doi.org/10.3748/wjg.v19.i17.2603.

40. Bishnoi, R., Hong, Y.R., Shah, C., Ali, A., Skelton, W.P., 4th, Huo, J., et al. (2019). Dipeptidyl peptidase 4 inhibitors as novel agents in improving survival in diabetic patients with colorectal cancer and lung cancer: a Surveillance Epidemiology and Endpoint Research Medicare study. Cancer Med. *8*, 3918–3927. https://doi.org/10.1002/cam4.2278.

41. Wang, Z., Ding, H., and Zou, Q. (2020). Identifying cell types to interpret scRNA-seq data: how, why and more possibilities. Brief. Funct. Genomics *19*, 286–291. https://doi.org/10.1093/bfgp/elaa003.

42. Ianevski, A., Giri, A.K., and Aittokallio, T. (2022). Fully-automated and ultra-fast cell-type identification using specific marker combinations from single-cell transcriptomic data. Nat. Commun. *13*, 1246. https://doi.org/10.1038/s41467-022-28803-w.

43. Choi, J.-H., In Kim, H., and Woo, H.G. (2020). scTyper: a comprehensive pipeline for the cell typing analysis of single-cell RNA-seq data. BMC Bioinf. *21*, 342. https://doi.org/10.1186/s12859-020-03700-5.

44. Pasquini, G., Rojo Arias, J.E., Schäfer, P., and Busskamp, V. (2021). Automated methods for cell type annotation on scRNA-seq data. Comput. Struct. Biotechnol. J. *19*, 961–969. https://doi.org/10.1016/j.csbj.2021.01.015.

45. Enserink, J.M., and Kolodner, R.D. (2010). An overview of Cdk1-controlled targets and processes. Cell Div. *5*, 11. https://doi.org/10.1186/1747-1028-5-11.

46. Castro, A., Bernis, C., Vigneron, S., Labbé, J.C., and Lorca, T. (2005). The anaphase-promoting complex: a key factor in the regulation of cell cycle. Oncogene *24*, 314–325. https://doi.org/10.1038/sj.onc.1207973.

47. Clark, A.J., Rosenberg, E.H., Almeida, L.S., Wood, T.C., Jakobs, C., Stevenson, R.E., Schwartz, C.E., and Salomons, G.S. (2006). X-linked creatine transporter (SLC6A8) mutations in about 1% of males with mental retardation of unknown etiology. Hum. Genet. *119*, 604–610. https://doi.org/10.1007/s00439-006-0162-9.

48. Mackenzie, B., Takanaga, H., Hubert, N., Rolfs, A., and Hediger, M.A. (2007). Functional properties of multiple isoforms of human divalent metal-ion transporter 1 (DMT1). Biochem. J. *403*, 59–69. https://doi.org/10.1042/BJ20061290.

49. Williams, J.M., Duckworth, C.A., Burkitt, M.D., Watson, A.J.M., Campbell, B.J., and Pritchard, D.M. (2015). Epithelial cell shedding and barrier function: a matter of life and death at the small intestinal villus tip. Vet. Pathol. *52*, 445–455. https://doi.org/10.1177/0300985814559404.

50. Blanchard, J.M. (2014). To be or not to be a proliferation marker? Oncogene *33*, 954–955. https://doi.org/10.1038/onc.2013.19.

51. Xu, H., Ghishan, F.K., and Kiela, P.R. (2018). SLC9 gene family: function, expression, and regulation. Compr. Physiol. *8*, 555–583. https://doi.org/10.1002/cphy.c170027.

52. Nikolovska, K., Seidler, U.E., and Stock, C. (2022). The role of plasma membrane sodium/hydrogen exchangers in gastrointestinal functions: proliferation and differentiation, fluid/electrolyte transport and barrier integrity. Front. Physiol. *13*, 899286. https://doi.org/10.3389/fphys.2022.899286.

53. Dudeja, P.K., Rao, D.D., Syed, I., Joshi, V., Dahdal, R.Y., Gardner, C., Risk, M.C., Schmidt, L., Bavishi, D., Kim, K.E., et al. (1996). Intestinal distribution of human Na+/H+ exchanger isoforms NHE-1, NHE-2, and NHE-3 mRNA. Am. J. Physiol. *271*, G483–G493. https://doi.org/10.1152/ajpgi.1996.271.3.G483.

54. Chandra, S.H.V., Wacker, I., Appelt, U.K., Behrens, J., and Schneikert, J. (2012). A common role for various human truncated adenomatous polyposis coli isoforms in the control of beta-catenin activity and cell proliferation. PLoS One *7*, e34479. https://doi.org/10.1371/journal.pone.0034479.

55. Klijn, C., Durinck, S., Stawiski, E.W., Haverty, P.M., Jiang, Z., Liu, H., Degenhardt, J., Mayba, O., Gnad, F., Liu, J., et al. (2015). A comprehensive transcriptional portrait of human cancer cell lines. Nat. Biotechnol. *33*, 306–312. https://doi.org/10.1038/nbt.3080.

56. Nestorowa, S., Hamey, F.K., Pijuan Sala, B., Diamanti, E., Shepherd, M., Laurenti, E., Wilson, N.K., Kent, D.G., and Göttgens, B. (2016). A single-cell resolution map of mouse hematopoietic stem and progenitor cell differentiation. Blood *128*, e20–e31. https://doi.org/10.1182/blood-2016-05-716480.

57. Qiu, X., Mao, Q., Tang, Y., Wang, L., Chawla, R., Pliner, H.A., and Trapnell, C. (2017). Reversed graph embedding resolves complex single-cell trajectories. Nat. Methods *14*, 979–982. https://doi.org/10.1038/nmeth.4402.

58. Subramanian, A., Tamayo, P., Mootha, V.K., Mukherjee, S., Ebert, B.L., Gillette, M.A., Paulovich, A., Pomeroy, S.L., Golub, T.R., Lander, E.S., and Mesirov, J.P. (2005). Gene set enrichment analysis: a knowledge-based approach for interpreting genome-wide expression profiles. Proc. Natl. Acad. Sci. USA *102*, 15545–15550. https://doi.org/10.1073/pnas.0506580102.

STAR★METHODS

KEY RESOURCES TABLE

REAGENT or RESOURCE	SOURCE	IDENTIFIER
Antibodies		
Mouse monoclonal anti-MUC13	Abcam	Cat#ab231158
Rabbit monoclonal anti-CDK1	Abcam	Cat#ab133327; RRID: AB_11155333
Rabbit polyclonal anti-Cyclin B1	Cell Signaling Technology	Cat#4138T
Rabbit polyclonal anti-DMT1	Abcam	Cat#ab123085; RRID: AB_10971807
Rabbit polyclonal SLC6A8	ThermoFisher Scientific	Cat#PA5-98276; RRID: AB_2812889
DyLight 488-conjugated goat anti-mouse antibody	Abcam	Cat#ab96871; RRID: AB_10680543
Alexa Fluor 555-conjugated goat anti-rabbit antibody	Abcam	Cat#ab150078; RRID: AB_2722519
Chemicals, peptides, and recombinant proteins		
SYLGARD 184 Silicone Elastomer Kit	Dow Corning	Cat#4019862
Rat tail collagen type I	Gibco	Cat#A10483-01
Matrigel	Corning	Cat#356235
Paraformaldehyde, 4% in PBS	Thermo Scientific	Cat#J19943.K2
Triton X-100	VWR International	Cat#97062-208
CruzFluor 647 conjugated phalloidin	Santa Cruz Biotechnology	Cat#sc-363797
4′,6-diamidino-2-phenylindole dihydrochloride	Thermo Scientific	Cat#62248
Bovine serum albumin	Cytiva	Cat#SH30574.02
Deposited data		
Raw and analyzed data	This paper	GEO: GSE199796
Experimental models: Cell lines		
Human: Caco-2 BBE	Harvard Digestive Disease Center	N/A
Software and algorithms		
GraphPad Prism	GraphPad Software	https://www.graphpad.com/
LAS X	Leica Microsystems	https://www.leica-microsystems.com/products/microscope-software/p/leica-las-x-ls/
IMARIS	Oxford Instruments	https://imaris.oxinst.com/
ImageJ	National Institute of Health	https://imagej.nih.gov/ij/
Cell Ranger	10x Genomics	https://support.10xgenomics.com/single-cell-gene-expression/software/downloads/latest
Seurat 3.0	Stuart et al.,[12]	https://satijalab.org/seurat/

RESOURCE AVAILABILITY

Lead contact

Further information and requests for resources and reagents should be directed to and will be fulfilled by the Lead Contact, Hyun Jung Kim (kimh19@ccf.org).

Materials availability

Materials generated in this study are available from the lead contact with a completed Materials Transfer Agreement.

Data and code availability

- The raw data in this study was deposited to Gene Expression Omnibus of the National Center for Biotechnology Information, with the accession number, GSE199796.
- This paper does not report original code.
- Any additional information required to reanalyze the data reported in this paper is available from the lead contact upon request.

EXPERIMENTAL MODEL AND SUBJECT DETAILS

Caco-2 BBE line (Harvard Digestive Disease Center) used in this study was routinely cultured in a T75 culture flask using Dulbecco's Modified Eagle medium (DMEM; Gibco) supplemented with 20% (v/v) fetal bovine serum (FBS, heat inactivated; Gibco) and antibiotics (100 U/mL penicillin, 100 μg/mL streptomycin, final concentration; Gibco) at 37°C under 5% CO_2. The cell line is originally derived from a male donor.

METHOD DETAILS

Microfabrication of a gut-on-a-chip

A gut-on-a-chip device was fabricated using polydimethylsiloxane (PDMS; SYLGARD 184 silicone elastomer kit, Dow Corning) by following general soft lithography method.[11] Briefly, silicon molds that are patterned with SU-8 (Microchem) with the designs of upper (1 mm in width, 10 mm in length, and 500 μm in height) and lower microchannels (1 mm in width, 10 mm in length, and 200 μm in height) of a gut-on-a-chip were prepared via a photolithography method. A silicon mold that has an array of pillars (10 μm in diameter, 25 μm in height, and 25 μm in spacing) was used to fabricate a PDMS porous membrane. Uncured PDMS mixture was prepared by vigorously mixing base silicone polymer and curing agent (15:1, w/w) and degassing it in a vacuum desiccator at room temperature for 20 min. Degassed PDMS mix was then poured on the silicon molds with target thicknesses of 7 and 1 mm for making an upper and a lower microchannel layer, respectively, then cured in a dry oven at 60°C for >4 h. To fabricate a porous membrane layer, ~1 mL of uncured degassed PDMS mix was poured on a membrane wafer, spread, and covered with a sheet of fluoropolymer-coated polyester film (3M Scotchpak Release Liner, 3M), then pressed with a weight (3 kg) while curing in a dry oven at 60°C for >6 h. After punching holes (diameter, 2 mm) in an upper layer for connecting silicone tubing, the upper layer was sequentially bonded to a membrane layer followed by a lower microchannel layer using a handheld corona treater (Electro-Technic). A complete gut-on-a-chip device was connected with silicon tubing (Tygon 3350; Saint-Gobain), sterilized with 70% ethanol, and dried in a dry oven at 60°C for overnight until use.

Culture of Caco-2 cells in a transwell and a gut-on-a-chip

To culture Caco-2 cells in a Transwell insert, dissociated Caco-2 cells (final density, 1×10^6 cells/mL) were seeded on the porous insert (0.4 μm in pores; Corning) pre-coated with a mixture of extracellular matrix solution (ECM; 100× diluted Matrigel (Corning) and 30 μg/mL of collagen type I (Gibco)) and incubated in a humidified CO_2 incubator at 37°C by changing culture medium every other day. Once the cells formed a confluent monolayer, cells were further cultured for 5 days. To culture Caco-2 cells in a gut-on-a-chip, the surface of microchannels in a fabricated device was activated with ultraviolet/ozone treatment for 40 min (UVO, Zelight Company Inc.), then coated with the same ECM mixture (Matrigel and collagen I) that we used in the Transwell culture in a humidified CO_2 incubator at 37°C for 1 h. After the ECM solution in the microchannels was replaced with a serum-containing culture medium, dissociated Caco-2 cells (final density, 1×10^7 cells/mL) were seeded in the upper microchannel and incubated in a humidified CO_2 incubator at 37°C for 1 h for cell attachment. Unbound cells were washed by flowing the culture medium and flow in the upper channel was maintained (volumetric flow rate at 30 μL/h, shear stress at 0.02 dyne/cm^2) until the cells form a confluent monolayer (24–36 h). The culture was further maintained under flow in both upper and lower microchannels at a flow rate of 50 μL/h and rhythmical stretching motions (10% strain, 0.15 Hz frequency) for 5 days.

Sample preparation for scRNA-seq analysis

To harvest the cells cultured in the Transwell, three inserts were washed with phosphate buffered saline (PBS, Ca^{2+}- and Mg^{2+}-free; Gibco) and treated with 200 μL of pre-warmed trypsin/EDTA (0.25% Trypsin and 0.913 mM EDTA; Gibco) for cell detachment at 37°C for 5 min. Cells were collected in a 15 mL conical tube, then mixed with 5 mL of serum-containing cell culture medium to inactivate trypsin. The dissociated cell suspension was filtered through a 20 μm cell strainer (pluriSelect) to remove cell clumps, and

centrifuged at 300×*g* at 4°C for 3 min. The cell pellet was then resuspended in 500 μL of freezing medium (10%, v/v, dimethyl sulfoxide in FBS), frozen at −80°C in a cell freezing container, and kept in liquid nitrogen until use. To harvest cells from the gut-on-a-chip culture, the channels were washed with 500 μL of PBS, and incubated with 300 μL of pre-warmed trypsin/EDTA at 37°C for 5 min. The dissociated cell suspension was collected in a 15 mL conical tube and incubated with 5 mL of a serum-containing cell culture medium for trypsin inactivation. The dissociated cells were filtered through a 20 μm cell strainer (pluriSelect) to remove cell clumps, centrifuged at 300×*g* at 4°C for 3 min, resuspended in 500 μL of freezing medium, then stocked in liquid nitrogen. For library preparation, the frozen cells were thawed and resuspended in 10 mL of 2% (w/v) bovine serum albumin (BSA; MP Biomedicals) dissolved in PBS. Cells were then washed by repeating centrifugation (300×*g*, 4°C, for 3 min), aspiration, and resuspension (in 500 μL of 2% BSA solution). Cell suspensions were run through the Chromium (10x Genomics) using the Single Cell 3′ Reagent Kits v3, following the manufacturer's protocol. The library-prepared samples were run for sequencing on the Illumina HiSeq Series with 50,000 target reads per cell.

Image analysis

Cell morphologies were routinely monitored by phase contrast microscopy (DMi1, Leica Microsystems). To visualize the contour of cell morphology formed in a Transwell insert and a gut-on-a-chip, we fixed the cells with 4% (w/v) paraformaldehyde (PFA; Alfa Aesar) for 10 min, permeabilized with 0.3% (v/v) Triton X-100 (VWR International) for 10 min, and stained with a mixture of CruzFluor 647 conjugated phalloidin (for F-actin; Santa Cruz Biotechnology) and 4′,6-diamidino-2-phenylindole dihydrochloride (DAPI for nuclei; final concentration, 1 μg/mL; Thermo Scientific) for 30 min, sequentially at room temperature under light protection. In each step, cells were rinsed with PBS to remove residual reagents.

To perform antibody-based immunofluorescence staining, cells were fixed (4% PFA, 10 min), permeabilized (0.3% Triton X-100 in 2% BSA, 30 min), and blocked (2% BSA, 1 h) at room temperature. Between steps, cells were washed with PBS. Primary antibody solutions (mouse monoclonal anti-MUC13, 10 μg/mL, Abcam; rabbit monoclonal anti-CDK1, 1:50 dilution, Abcam; rabbit polyclonal anti-Cyclin B1, 1:100 dilution, Cell Signaling Technology; rabbit polyclonal anti-DMT1, 4 μg/mL, Abcam; rabbit polyclonal SLC6A8, 1:50 dilution, ThermoFisher Scientific) were incubated with the cells at room temperature for 3 h. After washing the cells with PBS, secondary antibody solutions (DyLight 488-conjugated goat anti-mouse antibody, Abcam; Alexa Fluor 555-conjugated goat anti-rabbit antibody, Abcam) were incubated with the cells at room temperature in dark for 3 h. A mixture of CruzFluor 647 conjugated phalloidin (1× concentration) and DAPI (1 μg/mL, final concentration) was subsequently introduced for the counter staining of F-actin and nuclei, respectively, under light protection at room temperature for 30 min. Fluorescence imaging analysis was performed via a laser-scanning confocal microscope (DMi8, Leica Microsystems) using a 25× objective (NA 0.95, water immersion, Leica) coupled with the TCS SPE confocal system with solid state excitation laser sources of 405, 488, 532, and 635 nm and an Ultra high dynamic PMT detector. To investigate the spatial expression in a gut-on-a-chip, z-stacked images were rendered in 3D using a 3D module on LAS X (Leica Microsystems) followed by additional deconvolution and reconstructing process using IMARIS (Oxford Instruments). To analyze spatially localized fluorescence signals of the epithelial layers formed in gut-on-a-chip devices, the height of epithelial cells was measured from the 3D reconstructed images. The measured heights were divided into three sections (upper, middle, and lower) and the intensity of each section was quantified using ImageJ (Ver. 1.52i). The upper, middle, and lower regions were determined by the location from the epithelial surface to the 1/3 location (Upper), from the 1/3 to the 2/3 location from the epithelial surface (middle), and from the 2/3 location to the bottom (Lower). The measured intensity was transformed into the percent intensity for quantitation.

Mapping and aggregation

The sequence read files were imported to Cell Ranger count (v3.0, 10x Genomics) to align to the human reference and generate the unique molecular identifier (UMI) counts of gene-cell matrix by sample. After quality control, 3,920 and 1,348 cells were captured from the gut-on-a-chip and the Transwell, respectively. Then Cell Ranger 'aggr' was used to aggregate the UMI counts matrixes of the two samples with batch effect correction.[12]

Quality control and single-cell transcriptomic analyses

Using Seurat 3.0, quality control was performed on Cell Ranger filtered counts. The cells and genes meeting the following conditions were selected for analyses: i) a gene was detected at least in 3 cells; ii)

a cell contained more than 2,000 and less than 6,000 detectable genes; and iii) for a cell, the percentage of total mitochondrial gene UMI was less than 20%. Then, a global-scaling normalization ('logNormalize', scale factor is 10,000 by default) was performed and 200 highly variable features were listed. After cell cycle scoring, regression, and scaling of the data, variable features were used for principal component analysis (PCA) process.[56] The number of principal components was determined using a gene correlation matrix by the 'elbow' method. Based on the Shared Nearest Neighbor (SNN) method, cells were classified into distinct clusters on the dimensional reduction plots. Finally, the UMAP[13] was used for non-linear dimensional reduction to reveal transcriptional characteristics of distinct cellular clusters. For cell clustering and non-linear dimensional reduction, 13 statistically significant principal component (PC) dimensions were used.

Pseudotemporal trajectory analysis

The normalized and log-transformed gene-cell matrix from Seurat-processed data was imported to Monocle 2. The top 10 differential expressed genes of all the 4 cell clusters calculated by 'FindAllMakers' in Seurat were collected, then the genes that contained the GO term 'GO_CELL_CYCLE' were filtered out. Next, the rest were used as the ordering genes for cell trajectory analysis. Cells of TW1 were set as the root – time zero for the pseudotemporal trajectory analysis for the CHIP subclusters.[57]

Identification of marker genes and gene set enrichment analysis

'FindMarkers' in Seurat 3.0 was used for analyzing the average log fold changes between two cell clusters. After ranking the log-fold changes of all expressed genes, the gene set enrichment analysis (GSEA) was performed with C5 ontology gene sets (GO items) for the paired two groups - CHIP3 versus CHIP1 and CHIP2 and CHIP clusters versus TW1.[58]

Correction of batch effect, data normalization, and concatenation

Technical batch effects often occur in scRNA-seq libraries prepared for sequencing in different experiments. To establish meaningful cross-dataset comparisons, initial QC filtered data were normalized by total counts in all cells using the global-scaling linear regression method "LogNormalize" with default parameters in Seurat 3.0 to correct batch effects. For comparative purposes, data from independent replicates and different conditions were aggregated and standardized to the same sequencing depth, resulting in a concatenated gene-barcode matrix of all samples. To further improve the analysis, we also implemented dimensionality reduction to the input dataset for comparative analyses.

QUANTIFICATION AND STATISTICAL ANALYSIS

Statistical analysis in Figure 2E was performed using GraphPad Prism 9. To evaluate the statistical significance between groups, ordinary one-way analysis of variance (ANOVA) tests with multiple comparisons were performed. Error bars in the bar charts indicate standard error of the mean (SEM). Other statistical analyses were performed in Seurat 3.0.